Journal of Marine Research, 48, 677–700, 1990

Dissipative dynamics of western boundary currents

by Paola Cessi,[1,2] R. Vance Condie[3] and W. R. Young[2]

ABSTRACT

We investigate the steady barotropic circulation patterns driven by inflow-outflow boundary conditions on a rectangular β-plane domain. An inertial jet enters the domain in the southwest corner and a broad eastward outflow is prescribed at the eastern boundary. On the western wall there is no mass flux and no slip.

With weak viscosity, ν, the western boundary jet "overshoots" northward, beyond the latitude band of the eastern outflow. As the viscosity is reduced the length of this overshoot increases as $\nu^{-2/3}$, before the jet gradually peels away from the western wall, plunges southward and eventually turns eastward. Away from the wall the current forms a damped stationary Rossby wave, as described by Moore in 1963.

The initial northward overshoot and southward "plunge" is a distinct dynamical regime, and not merely the first and largest undulation of the Rossby wave. For instance the zonal length scale of the overshoot is just the Munk scale, $(\nu/\beta)^{1/3}$, and inertia, planetary vorticity and viscosity are all important at leading order in the dynamical balance as $\nu \to 0$. All of the streamlines pass through this dissipative region and most of the Lagrangian potential vorticity alterations occur here, rather than in the Rossby wave.

The preceeding scenario applies only when the northern boundary is distant, so that the overshoot peels away from the western wall before striking the northwest corner of the domain. If the jet reaches the northern boundary it drives an inertial recirculating gyre in the corner.

1. Introduction

In 1963 Moore proposed a simple and influential model of the terminus of the western boundary layer. In a subtropical gyre this is the northwest corner of the circulation, where the interior Sverdrup flow is to the east, and fluid that has been carried northward in the western boundary layer must return to this interior. Using an Oseen linearization about the eastward Sverdrup flow, Moore proposed that closure of the mass flux is achieved by a circulation pattern which is essentially a damped stationary Rossby wave. Pedlosky (1987) argues that the role of this undulation is to increase the length of a streamline and allow sufficient time for the low values of potential vorticity carried by the fluid leaving the boundary layer to diffuse out of the

1. Istituto FISBAT-CNR, I-40126, Bologna, Italy.
2. Scripps Institution of Oceanography, La Jolla, California, 92093, U.S.A.
3. Lamont Doherty Geological Observatory, Palisades, New York, 10964, U.S.A.

basin. In Pedlosky's interpretation the wave is analogous to a baffle that increases the efficacy of weak diffusion.

Moore's study was in the context of the steady barotropic model of the wind driven ocean circulation:

$$J(\psi, q) = \frac{f_0 w_E}{H} + \nu \nabla^2 q \quad \text{where } \mathbf{u} = \hat{\mathbf{z}} \times \nabla\psi \text{ and } q \equiv \beta y + \nabla^2\psi \tag{1.1}$$

(e.g. Hendershott, 1987; Pedlosky, 1987). Here ψ is the streamfunction for the geostrophic part of the velocity, q is the quasigeotrophic potential vorticity, w_E is the Ekman pumping which is proportional to the wind-stress curl, ν is the lateral eddy viscosity and H is the layer thickness. The standard boundary conditions are no mass flux ($\psi = 0$) and no-slip ($\partial_n \psi = 0$ where n is the normal coordinate).

Despite the many idealizations in this model, and in Moore's study, it remains one of the few serious theoretical attempts to understand how dissipation acting on the general circulation balances the wind forcing. Pedlosky emphasizes this using the dissipation integrals (see his Section 5.9). An equally informative diagnostic is the global energy balance obtained by multiplying (1.1) by ψ and integrating over the area of the basin. The result is

$$\int \psi \frac{f_0 w_E}{H}\, dA = \nu \int \zeta^2\, dA \tag{1.2}$$

where $\zeta \equiv \nabla^2\psi$ is the relative vorticity. The order of magnitude of the left-hand side can be estimated using the interior Sverdrup balance, $\psi_S \sim a f_0 w_E/\beta H$ where a is the east-west length scale. The important point is that the production term on the left is independent of ν.

In the linear limit, when the forcing is weak or the viscosity is large, the western boundary layer closure is that described by Munk (1950) with thickness

$$\delta_M \equiv \left(\frac{\nu}{\beta}\right)^{1/3}. \tag{1.3}$$

In this limit the western boundary layer dissipates the energy input from the wind. (Notice that the right-hand side of (1.2) is independent of ν because in the boundary layer $\zeta^2 \sim \delta_M^{-4} \sim \nu^{-4/3}$ while the area of this region is proportional to $\delta_M \sim \nu^{1/3}$.)

In the nonlinear or "inertial" limit, when the forcing is strong or the viscosity small, the thickness of the boundary layer, in the region of westward interior flow, is the inertial scale

$$\delta_I \equiv \left(\frac{U_S}{\beta}\right)^{1/2} \tag{1.4}$$

found by Charney (1955) and Morgan (1956). Here U_S is the maximum speed of the westward Sverdrup flow impinging on the boundary layer. In this case, because the inertial boundary layer thickness is independent of ν, its contribution to the right-hand side of (1.2) is not sufficient to balance the left. Of course, the inertial boundary layer does not satisfy the no slip condition and so there is a viscous sublayer, of thickness $\delta_\nu \ll \delta_I$, to fulfill this condition. For the moment the essential point is that $\delta_\nu \sim \nu^{1/2}$ so that the contribution of the viscous sublayer to the right-hand side of (1.2) is proportional to $\nu^{1/2}$, and is also incapable of balancing the source on the left. This emphasizes that the primary role of the western boundary layer is to close the mass flux rather than to satisfy the no slip condition and balance dissipation budgets.

To summarize: in the inertial limit of the steady barotropic model, straightforward scale analysis shows that the boundary layers are not strong enough to dissipate the energy pumped into the large scale flow by the wind. Pedlosky reaches an analogous conclusion based on his consideration of the potential vorticity balance within a region enclosed by a streamline. He argues that the dissipation deficit is balanced in the damped stationary Rossby wave. It turns out that scale analysis based on the global energy balance leads to identical results so that apparently a consistent scenario emerges: the damped stationary Rossby wave is a localized region of dissipative activity required to balance both the potential vorticity and energy budgets in the barotropic circulation model. It is also the site of alterations in potential vorticity from the low values characteristic of where fluid entered the western boundary layer, to the higher values of the northern Sverdrup interior.

Moore's model has been questioned by a number of authors and we present a detailed summary of their objections below. It is now clear from these publications that either a northern wall, or a strong northern gyre, prevents the formation of a damped stationary Rossby wave. Instead enhanced dissipation is associated with an inertial recirculation (Cessi *et al.*, 1987) whose strength increases as viscosity decreases. However an important conclusion of this article is that if a boundary current somehow separates far away from the northern wall then the resulting flow exhibits Moore's damped Rossby wave far away from the western boundary. In the present article we induce separation in a steady barotropic regional model by simply imposing an eastward interior flow well south of the northern boundary. The distinction between recirculation and Moore's scenario is important from an observational perspective because the recirculation gyres significantly augment the eastward transport of the separated boundary current, while the train of damped Rossby waves does not.

In collaboration with G.R. Ierley we have also seen examples of separation in eddy resolving general circulation models. In these simulations instabilities in the western boundary layer (e.g. Ierley and Young, 1990) cause the current to leave the coast south of the northern gyre boundary. The mean fields show an unmistakable damped

stationary Rossby wave as the fluid leaving the boundary current flows back into the Sverdrup interior. Separation induced by time dependent instabilities is beyond the scope of the present article. Instead we confine attention to the damped stationary Rossby wave in its most elementary setting: the steady barotropic model.

a. Criticism of Moore's scenario. Objections to Moore's scenario first appeared in 1964 when its mathematical foundation was questioned by Il'in and Kamenkovich. This interesting study took as its point of departure an ordinary differential equation which is obtained by expanding the stream-function in a Taylor series about either the northern or the southern boundary of the basin. For instance suppose that the basin is a rectangle $0 < x < a$ and $0 < y < b$ and the Ekman pumping has the standard form for a subtropical gyre

$$\frac{f_0 w_E(y)}{H} = -\frac{f_0 W}{H} \sin\left(\frac{\pi y}{b}\right), \tag{1.5}$$

where the positive constant, W, is an Ekman pumping scale. The corresponding interior Sverdrup solution is

$$\psi_S(x, y) = \frac{f_0 W}{\beta H}(a - x) \sin\left(\frac{\pi y}{b}\right) \quad \text{so that } U_S \equiv \frac{\pi f_0 W_a}{\beta H b}, \tag{1.6}$$

where we recall that U_S is the maximum speed of the zonal Sverdrup flow—see (1.4). If the expansion is pivoted on the northern boundary one introduces $\hat{y} \equiv b - y$ and then

$$\psi = \hat{y}\phi_1(x) + \hat{y}^2\phi_2(x) + \cdots \tag{1.7}$$

Substituting this into (1.1) gives the leading order equation

$$\phi_1\phi_1'' - \phi_1'^2 + \beta\phi_1 = \sigma\beta U_S + \nu\phi_1''' \tag{1.8}$$

where the constant of integration on the right-hand side was determined by matching to the Sverdrup interior in (1.6) and $\sigma = +1$ if the expansion is about the northern boundary as in (1.7), and $\sigma = -1$ if about the southern. This is the "parametric model"—so called because it assumes that the y dependence of the boundary layer is weak or parametric. More details are given by Moore (1963), Il'in and Kamenkovich (1964), Ierley and Ruehr (1986), Ierley (1987) and Mallier (1989). This last reference discusses the higher order corrections ϕ_2 etc.

We emphasize that the parametric form in (1.7) assumes the existence of a wall at $y = b$ so that $\psi(x, b) = 0$. Conclusions based on this expansion do not apply to "open boxes" in which the flow is not constrained by such a barrier. It is precisely in this "open" geometry in which we find the Rossby wave.

Moore's Oseen approximation amounts to linearizing (1.8) about the interior

solution

$$\phi(x) \approx U_S + \epsilon(x) \tag{1.9}$$

so that if quadratic terms are neglected then ϵ satisfies a third order linear differential equation. This equation has two oscillatory solutions which are damped as $x \to \infty$. The implication is that the nonlinear equation (1.8) has a solution satisfying both the boundary conditions at the western wall, $\phi_1(0) = \phi_1'(0) = 0$, and the matching condition as x increases. The surprising conclusion of Il'in and Kamenkovich's numerical study of the full nonlinear problem in (1.8) is that this is incorrect if W is large enough and the expansion is around the northern wall ($\sigma = 1$). That is, if the forcing is sufficiently strong there is no solution of (1.8) in the outflow region which simultaneously satisfies the boundary conditions at the wall and matching conditions onto the Sverdrup interior.

In their study of the parametric model Il'in and Kamenkovich used no-slip ($\phi_1'(0) = 0$) on the wall as a boundary condition. Ierley and Ruehr (1986) in a comprehensive study of the solutions of (1.8) investigated both no slip and slip ($\phi_1''(0) = 0$) boundary conditions. There are no important qualitative differences between the two cases. In both cases if the forcing is sufficiently strong there is no solution satisfying the boundary and matching conditions. For no slip the critical value of the forcing in (1.8) is $U_S^{\text{crit}} = 0.79130\beta\delta_M^2$ while for slip $U_S^{\text{crit}} = 0.29657\beta\delta_M^2$.

Ierley (1987) studied this issue further using a regional model of the western boundary layer. He solved (1.1) with $w_E = 0$ in a rectangular domain ($0 < x < a$ and $0 < y < b$) with an inflow-outflow condition on the eastern "wall," $x = a = 10\delta_M$. On this open boundary he specified $\psi(a, y) = \psi_S(0, y)$ and $q(a, y) = \beta y + \partial_y^2\psi_S(0, y)$ where ψ_S is defined in (1.6). On the other three walls the boundary conditions are $\psi = \partial_n^2\psi = 0$ i.e., slip. There are two nondimensional parameters in this regional model. First there is λ[4]

$$\lambda \equiv -\left(\frac{U_S}{\beta\delta_M^2}\right) = -\left(\frac{\delta_I}{\delta_M}\right)^2, \tag{1.10}$$

which measures the strength of the forcing, and additionally there is a geometric ratio α:

$$\alpha \equiv \frac{b}{a} = \frac{b}{10\delta_M}. \tag{1.11}$$

Ierley showed that the boundary layer approximation, $\partial_x \gg \partial_y$, is valid only when the

4. λ defined here is a negative number that approaches $-\infty$ as the forcing, U_S, is increased. We adopt this unusual definition so that our notation agrees with the convention Ierley used in discussing the nondimensional form of (1.8). In that instance the one nondimensional parameter in the ordinary differential equation is $\lambda = -\sigma U_S/\beta\delta_M^2$. There are no solutions when $\sigma = 1$ and U_S is sufficiently large i.e. when λ is negative.

forcing is less than a certain critical value which is a function of the aspect ratio α. That is, the solution has boundary layer character if

$$\lambda > \lambda_{crit}(\alpha). \tag{1.12}$$

When this inequality is reversed the boundary layer approximation fails and a recirculating gyre, rather than a damped stationary Rossby wave, appears in the northwest corner of the domain. Ierley made contact with the parametric model by demonstrating that as $\alpha \to \infty$, λ_{crit} approaches the value given by the parametric model i.e. $\lambda_{crit}(\infty) = -0.29657$. This is further evidence against Moore's scenario—a complete solution of the partial differential equation does not exhibit the damped undulation. (Actually in Ierley's figures there are small spatial oscillations south of the gyre but there is only one, or at most two, crests.)

We emphasize that in Ierley's regional study the northern wall abuts the eastward outflow and suppresses the Rossby wave. In Section 2 we report calculations with this same regional model in which the center of the eastern outflow is shifted far south of the northern barrier. There is a stationary Rossby wave supported by the eastward flow.

As further evidence of the role of a northern barrier in preventing the appearance of a wave we note that numerical solutions of (1.1) with the forcing function in (1.5) reported by Böning (1986) and Cessi *et al.* (1987) clearly show a recirculating gyre in the northwest corner of the basin. There is no damped stationary Rossby wave. However in these calculations the boundary condition on the western wall is slip. Early calculations by Bryan (1963) and Blandford (1971) used no slip. But by modern standards these are rather strongly damped and it is difficult to support any firm conclusions about the nonlinear limit with them. It is true however that Bryan's more inviscid runs (for instance Fig. 5.11.1 in Pedlosky, 1987) exhibit both a small recirculating gyre and damped stationary Rossby waves, with perhaps two oscillations. A more recent and less viscous sequence of no slip calculations are those of Panteleev (1985). His figures clearly illustrate the existence of a nonlinear inertial gyre in the northwest corner of the basin. There is no extensive damped stationary Rossby wave and in fact the time-averaged circulation pattern is qualitatively similar to Böning's slip model.

Thus there appear to be no important qualitative differences between slip and no slip models forced by a single gyre wind stress curl such as (1.5) and with a wall at $y = b$. In both cases the dissipation required to satisfy the potential vorticity and energy budgets takes place in an inertial gyre (and in its northern boundary layer). And this same feature enhances the transport of the western boundary currents by an order of magnitude above that required to balance the mass flux from the linear Sverdrup interior; e.g., Cessi *et al.* (1987). In neither case is there any support for Moore's wave.

The various restrictions associated with this conclusion should be noted. We are considering a model that is

(i) quasigeostrophic and barotropic

(ii) steady

(iii) driven by a single gyre Ekman pumping, such as (1.5)

(iv) bounded to the north by a coast.

We accept the first two of these as the defining characteristics of an elementary and widely studied class of ocean models that is still not completely understood. The second two restrictions are less fundamental and in fact there is evidence in the literature that removing these allows the development of the stationary Rossby wave and suppresses recirculation. For instance Moro (1988) used an asymmetric, two gyre pattern of Ekman pumping to force (1.1). In his calculations, the maximum Ekman pumping in the subpolar gyre is about twice that in the subtropical gyre. Both slip and no slip boundary conditions were studied. With either boundary condition a distinct train of damped stationary Rossby waves develops at the boundary between the two gyres. Moro concludes that the similarity between this calculation and Moore's model is "only superficial." This is true in the sense that Moore based his argument on the linearization of (1.8), and the derivation of this ordinary differential equation relies crucially on (iii) and (iv) above. But it is easy to avoid these assumptions and directly linearize (1.1) to obtain essentially the same results (e.g., Pedlosky, 1987). Moro does not attempt to compare the results of his numerical model with Pedlosky's scale analysis. Some rough calculations, based on estimating the wavelength from Moro's figures, indicate that the train of undulations is probably the damped stationary Rossby wave predicted by Moore. Specifically the estimated wavelength is consistent with Moore and Pedlosky's value $2\pi\delta_I$.

To summarize this review: in the inviscid limit of the steady, barotropic, wind driven model there are two different circulation patterns that return the fluid from the western boundary layer to the Sverdrup interior. There is the damped stationary Rossby wave, described first by Moore and seen clearly in Moro's calculations, and there is the inertial recirculation, exhibited in Böning's calculations and modelled theoretically by Cessi *et al.* (1987). In the presence of a northern wall (or of a subpolar gyre whose strength is comparable to the subtropical gyre) the Rossby wave pattern is suppressed and gives way to the inertial gyre pattern.

2. A regional model

The regional model we use is shown schematically in Figure 1 and described in more detail by Ierley (1987). Essentially it solves (1.1) using Newton's method. We take $w_E = 0$ and force the flow by imposing inflow-outflow boundary conditions on the sides

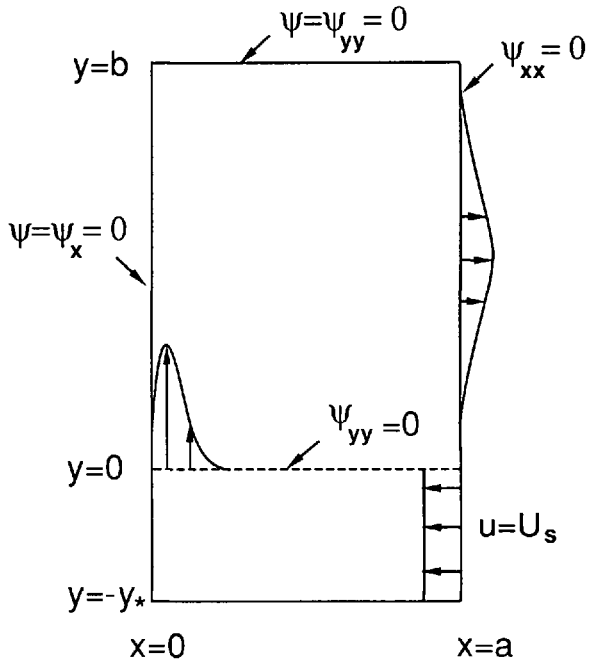

Figure 1. A schematic of the regional model. The computational domain is $b > y > 0$. The flow in the southern region, $0 > y > -y_*$, is found from (1.8) with $\sigma = -1$. The result from this ordinary differential equation is used to specify a dynamically consistent inflow along the line $y = 0$.

of a rectangular domain. The resulting steady solution may be unstable to time dependent disturbances, but this issue is outside the scope of the present study.

On the southern boundary, $y = 0$, we impose the streamfunction and its second derivative

$$\psi(x, 0) = y_*\phi_1(x) \quad \text{and} \quad \psi_{yy}(x, 0) = 0 \tag{2.1}$$

where ϕ_1 is a solution of (1.8) with $\sigma = -1$. Thus the total transport flowing into the domain is

$$\Phi \equiv U_S y_*. \tag{2.2}$$

The inflow velocity obtained from (2.1) is shown in Figure 2. In using the solution of (1.8) as a boundary condition for the regional model we are envisaging the configuration shown in Figure 1 where in the southern region, $-y_* < y < 0$, a uniform inflow, U_S, impinges on the western wall and drives a viscous-inertial boundary layer northwards. The parametric model, (1.8), provides an exact solution of the equations of motion so that it is not necessary to explicitly model the westward inflow with the regional model.

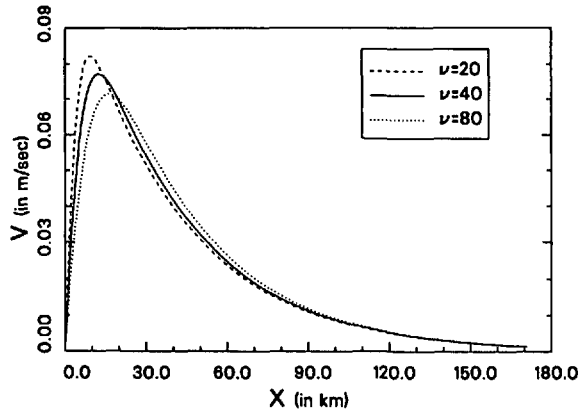

Figure 2. Three examples of the northward velocity obtained from (2.1) and (1.8) with various values of ν in mks. In all cases $U_S = 0.0325$ mks and $y_* = 120.9$ km so that $\delta_I = 40.3$ km and $v_{max} \to 3U_S$ as $\nu \to 0$. The outer inertial region in which (2.6) applies is evident.

Instead the computational domain of the regional model is $0 < y < b$ in which the outflow is specified over a portion of the eastern, open boundary.

We originally experimented with analytic expressions for the southern boundary condition, $\psi(x, 0)$, as alternatives to solving (1.8) (e.g., Condie, 1989). We discovered that satisfactory reduction of residual error in the solution of the regional model requires that the boundary condition satisfy certain constraints which can be deduced from the equation of motion. For instance, Stewart (1964) noted that within the context of the boundary layer approximation one has $\nu\psi_{xxx}(0, y) = -\beta\psi(\infty, y)$. And there are several other conditions on the boundary which can be deduced from the equations of motion, especially if one assumes that $\zeta \approx \psi_{xx}$. Building all of these into an analytic form is cumbersome and ultimately it was simplest, both conceptually and practically, to use the solutions of (1.8) instead of analytic forms.

As a concrete example of a choice of parameters in (2.1) and (2.2) our "pivot" case is

$$U_S = 0.0325\ \text{ms}^{-1},\quad \beta = 2 \times 10^{-11}\text{m}^{-1}\text{s}^{-1},\quad y_* = 120.9\ \text{km},\quad \nu = 20\ \text{m}^2\text{s}^{-1}, \tag{2.3}$$

for which the boundary layer length scales in (1.3) and (1.4), and the transport in (2.2), are

$$\delta_I = 40.3\ \text{km},\quad \delta_M = 10.0\ \text{km}\quad \text{and}\quad \Phi = 3{,}930\ \text{m}^2\text{s}^{-1}. \tag{2.4}$$

The domain size in the pivot case is

$$0 < x < a = 750\ \text{km}\quad \text{and}\quad 0 < y < b = 1{,}300\ \text{km}. \tag{2.5}$$

Figure 2 shows the velocity profile obtained from numerical solution of (1.8). There is

an outer inertial region in which

$$v(x, 0) = y_* \frac{d\phi_1}{dx} \approx \frac{U_S y_*}{\delta_I} e^{-x/\delta_1}, \tag{2.6}$$

and an inner viscous sublayer of width

$$\delta_v \equiv \left(\frac{\delta_M^3}{\delta_I}\right)^{1/2}, \tag{2.7}$$

which for the pivot is approximately 5 km.

On the western boundary we impose both no mass flux ($\psi = 0$) and no-slip ($\psi_x = 0$). On the northern boundary we impose no mass flux ($\psi = 0$) and slip ($\psi_{yy} = 0$).

On the eastern wall we specify an outflow centered on $Y < b$. Specifically we use the functional form[5]

$$\psi(a, y) \approx \frac{\Phi}{2}\left[1 - \tanh\left(\frac{y - Y}{l}\right)\right] \tag{2.8}$$

and for the pivot

$$Y = 650 \text{ km} \quad \text{and} \quad l = 290 \text{ km}. \tag{2.9}$$

The zonal velocity corresponding to (2.8) is

$$u(a, y) = -\psi_y(a, y) = U_{\max} \operatorname{sech}^2\left(\frac{y - Y}{l}\right) \text{where } U_{\max} \equiv \frac{\Phi}{2l}. \tag{2.10}$$

We anticipate the existence of a stationary Rossby wave supported by this eastward zonal flow. According to Moore's scaling this wave has an inverse wavenumber of order

$$\delta_{RW} \equiv \sqrt{\frac{U_{\max}}{\beta}}. \tag{2.11}$$

For the pivot case $U_{\max} = 6.776 \times 10^{-3}$ m s^{-1} and $\delta_{RW} = 18.4$ km.

The second boundary condition at the eastern boundary is

$$\psi_{xx}(a, y) = 0. \tag{2.12}$$

We choose Φ and l so that the shear, ψ_{yy}, is weak and consequently on the eastern boundary $q \approx \beta Y$.

5. Equation (2.8) is approximate because we also included a term linear in y, with an exponentially small coefficient, to ensure that ψ was continuous at the northeast and southeast corners. This is necessary because $\phi_1(a)$ in (2.1) differs from its asymptotic value, Φ, by an exponentially small term.

Table 1. Parameters for the computations. In all cases $\beta = 2 \times 10^{-11}$ mks and the domain size is as in (2.5). We also take $y_* = 3\delta_I$ so that $\delta_I = (\Phi/3\beta)^{1/3}$. The eastern outflow is always given by (2.9) and (2.10).

	ν (mks)	Φ (mks)	$\hat{\nu} \equiv (\delta_M/\delta_{RW})^3$	δ_I/δ_M	$2\delta_{RW}^4/\delta_M^3$ (km)
Run 1	20	3,930	0.1603	4.031	229.6
Run 2	40	3,930	0.3207	3.199	114.8
Run 3	160	15,720	0.1603	3.199	459.2
Run 4	15	3,930	0.1203	4.436	306.1

3. Results

a. An overview of the numerical results. Table 1 summarizes the parameters used in four different solutions. The pivot is run 1 and is shown in Figure 3. There is an unmistakable oscillation away from the wall. Immediately adjacent to the wall there is a large amplitude northward "overshoot" followed by a southward "plunge." We argue below that this first loop is a distinct dynamical regime, and not just the first and largest undulation of the damped Rossby wave. For the moment we emphasize that the zonal scale of this loop is δ_M, while that of the damped wave in the interior is $\delta_{RW} \gg \delta_M$.

In Figure 4 ν has been doubled. Both the "overshoot" and the "plunge" become less pronounced as ν is increased, and the wave does not extend as far east.

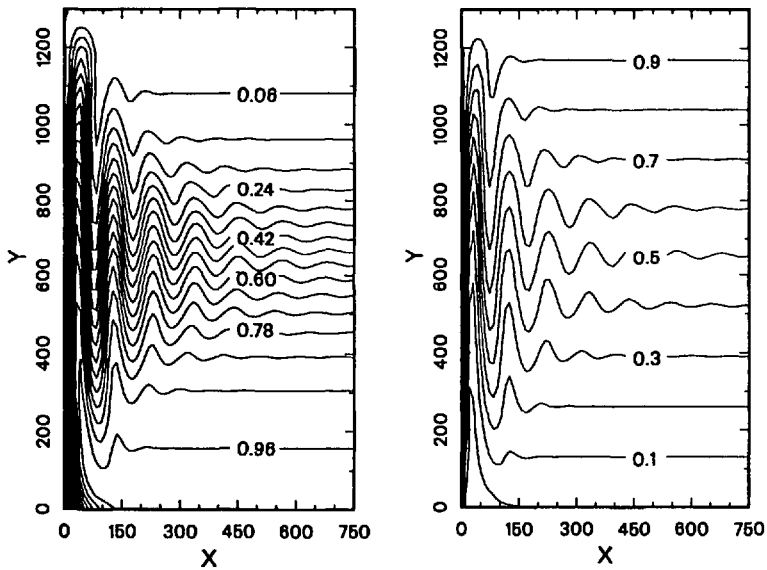

Figure 3. This figure shows the streamfunction and potential vorticity of the pivot case (run 1 in Table 1). The damped stationary wave on the outflow is unmistakable and its eastward penetration decreases when the viscosity is increased (Fig. 4). Near the wall a large amplitude loop (the northward "overshoot" and the southward "plunge") is obtained.

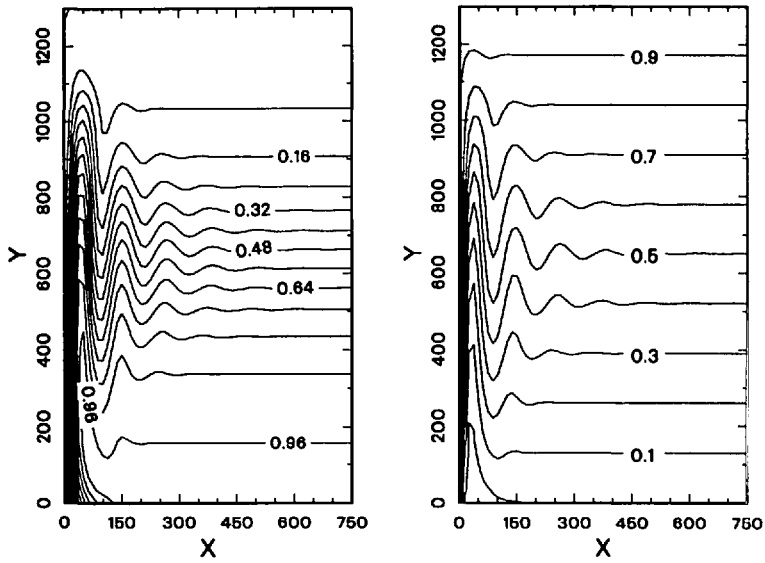

Figure 4. Shown are the streamfunction and potential vorticity of run 2 from Table 1. The increase in viscosity from run 1 decreases both the amplitude of the first loop of the boundary current and the eastward penetration of the stationary wave.

Figure 5 shows the streamfunction and potential vorticity of run 3 as solid lines. In run 3 the transport has been increased by a factor of four relative to that in run 1 and the viscosity by a factor of eight. Thus δ_M and δ_{RW} are larger by a factor of two, and there is no longer good scale separation between the damped wave and the box. In particular we believe that the eastern boundary condition is probably intrusive because it forces the wave to satisfy a quantization condition at $x = a$.

Also shown in Figure 5 as a dashed line is the streamfunction and potential vorticity from Figure 3. In anticipation of future remarks about the scales of the damped wave we note that in Figure 5 δ_{RW} has been used to scale zonal lengths. Thus only the westernmost 368 km of the domain from Figure 3 is shown in Figure 5.

Figure 6 shows the streamfunction and potential vorticity of run 4. We have already noted in Figures 3 and 4 that decreasing ν results in a larger "overshoot" before the boundary current separates from the wall. In Figure 6 we see that if the jet reaches the northern wall before separation it drives an inertial gyre in the corner. From our experience with wind-driven models we anticipate that if ν were decreased further the recirculating gyre would become a dominant feature and expand in the zonal direction. Moreover, as viscosity is reduced, the transport recirculated in this compact gyre increases and eventually exceeds Φ. We have not been able to decrease diffusion beyond $\nu = 15$ mks because already at this viscosity the damped Rossby wave reaches the eastern wall and its wavelength is affected by a quantization condition. This could be avoided by increasing the size of the basin and the resolution. Unfortunately Newton

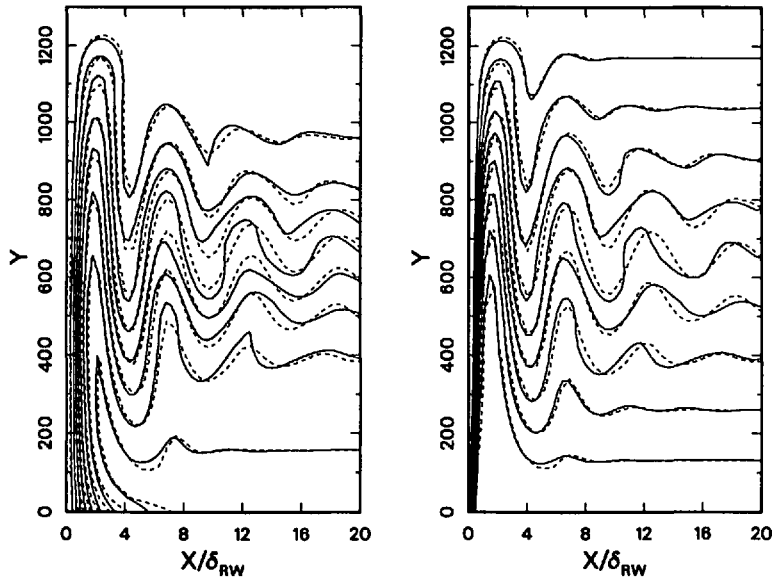

Figure 5. The solid curve is the streamfunction and potential vorticity corresponding to run 3. In this figure the x-axis is scaled in units of δ_{RW}. (For run 3 $\delta_{RW} = 36.8$ km so that $20\,\delta_{RW} = 736$ km $\approx a = 750$ km.) The dashed curve is run 1 for which $20\,\delta_{RW} = 368$ km.

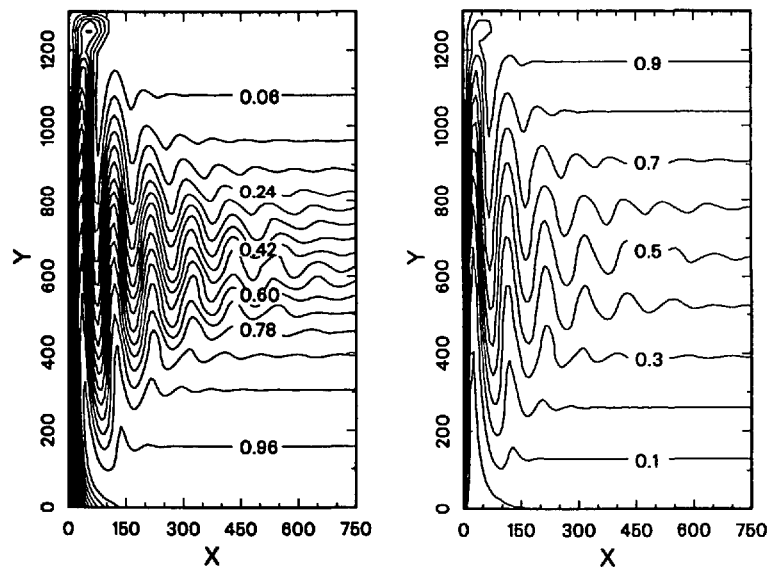

Figure 6. Shown are the streamfunction and potential vorticity of run 4 from Table 1. The transport is the same as in Figure 3, but the decrease in viscosity increases the overshoot so that the boundary current "finds" the northern wall and forms an inertial gyre.

method requires the inversion of a matrix whose size increases as the square of the number of Chebyshev polynomials in each direction. For run 4 we use 89 polynomials in x and 51 in y so that the memory requirement is roughly 16 megawords. Further increases in resolution are prohibitively expensive.

b. The boundary layer approximation and integral constraints. Because of the evident disparity between the x and y scales in Figures 3 and 4 we use the boundary layer approximation, $q \approx \beta y + \psi_{xx}$. In this case (1.1) with $w_E = 0$ can be written as

$$\partial_x J(\psi, \psi_x) + \beta\psi_x = \nu\psi_{xxxx}, \tag{3.1}$$

and then integrated so that

$$J(\psi, \psi_x) + \beta\psi - \beta\phi = \nu\psi_{xxx}, \tag{3.2}$$

where $\phi(y) \equiv \psi(a, y)$ is given by (2.8). Eq. (3.2) can be put a more revealing form as

$$uv_x + vv_y + \beta(\psi - \phi) = \nu v_{xx}, \tag{3.3}$$

which is the y momentum equation at first order in the standard Rossby number expansion. This form is useful because it is similar to the classic boundary layer equation (with $-\beta\phi(y)$ playing the role of an external pressure gradient) discussed for instance in Batchelor (1967) and Schlichting (1979). Many of the results developed in that context are applicable to (3.3), but the extra term $\beta\psi$ has important consequences such as the stationary Rossby wave in the earlier figures.

An important result, which helps us understand the numerical calculations, is obtained by evaluating (3.2) at $x = 0$:

$$\nu\psi_{xxx}(0, y) = \nu q_x(0, y) = -\beta\phi(y). \tag{3.4}$$

This is Stewart's (1964) constraint. It shows that the diffusive flux of potential vorticity through the western boundary is known in terms of the imposed outflow on the eastern open boundary. In the calculations shown in Figures 3 and 4 this result is satisfied very accurately which is strong evidence in support of the boundary layer approximation in (3.2).

The result in (3.4) is interpreted physically as a constraint on the potential vorticity fluxes. Consider a control region defined by the area south of a particular latitude, y. It is easy to see that the advective flux of potential vorticity through the southern boundary, $y = 0$, into the control area vanishes. With no slip boundary conditions, the advective flux of potential vorticity through the northern boundary, y, of this control region is

$$\int_0^a v(\beta y + v_x)\, dx \approx \beta y\phi(y). \tag{3.5}$$

The advective flux out of the control region at the eastern boundary, $x = a$, is

$$\int_0^y \beta y_1 u(a, y_1)\, dy_1 = -\beta y \phi(y) + \beta \int_0^y \phi(y_1)\, dy_1. \tag{3.6}$$

The remaining flux into the control region is the diffusive flux through the western wall and from (3.4) we see that the three nonzero fluxes sum to zero.

To complete this subsection we briefly obtain the momentum and energy fluxes from (3.2). Integrating from $x = 0$ to $x = a$ one has the momentum constraint

$$\partial_y \int_0^a v^2\, dx + \beta \int_0^a (\psi - \phi)\, dx = -\nu\zeta(0, y). \tag{3.7}$$

The first term is the divergence of the flux of meridional momentum. The second term, proportional to β, is the Coriolis torque on the ageostrophic part of the velocity. The final term is the viscous stress on the wall.

The energy balance is obtained by multiplying (3.2) by $v = \psi_x$ and then integrating across the domain from $x = 0$ to $x = a$. The result is

$$\partial_y \int_0^a (v^3/2)\, dx = (\beta\phi^2/2) - \nu \int_0^a v_x^2\, dx. \tag{3.8}$$

The first term is the divergence of the energy flux, the second is the pressure work from the boundary, and the final is the viscous dissipation.

c. Scaling of the Rossby wave regime. We now turn to some scaling arguments for the flow in Figures 3 and 4. We distinguish between the interior damped wave and the loop current immediately adjacent to the wall. We first discuss the wave and following Moore and Pedlosky we adopt the following scaling

$$x = \delta_{RW}\hat{x}, \quad y = l\hat{y}, \quad (\psi, \phi) = \Phi(\hat{\psi}, \hat{\phi}), \quad \hat{\nu} \equiv \frac{\delta_M^3}{\delta_{RW}^3} = \frac{\nu\beta^{1/2}}{U_{\max}^{3/2}}. \tag{3.9}$$

In (3.9) l is the meridional scale of the eastern outflow in (2.8) and δ_{RW} is defined in (2.11). Suppressing most of the hats the nondimensional equation is

$$J(\psi, \psi_x) + \psi - \phi = \hat{\nu}\psi_{xxx}. \tag{3.10}$$

We believe that (3.9) is an appropriate choice of scales for the wavy region, far away from the western wall. Thus there is only one controlling nondimensional parameter, $\hat{\nu}$. Other nondimensional parameters which might be inherited from the southern inflow, such as δ_I/δ_M, do not affect the structure of the wave. In support of this assertion we show in Figure 5 a comparison of run 1 with 3 after rescaling with (3.9). The coincidence of the contours is evidence that δ_{RW} is the correct zonal length scale. This confirms Moore's and Pedlosky's scaling argument in the region near the outflow.

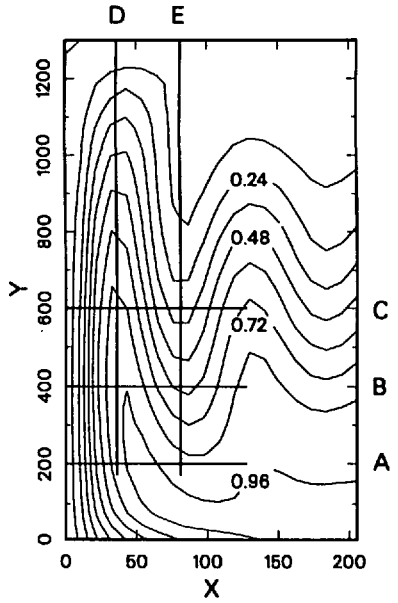

Figure 7. Superimposed on an expanded view of the western region of Figure 3 are five sections used for model diagnostics.

d. Scaling of the loop current. In the vicinity of the wall diffusion is important and we suggest that the following scaling is appropriate in this region:

$$x = \delta_M \hat{x}, \quad y = \mathcal{L}\hat{y}, \quad (\hat{\psi}, \hat{\phi}) = \Phi(\psi, \phi), \quad \mathcal{L} \equiv l\frac{\delta_{RW}^2}{\delta_M^2} = \frac{\Phi}{\beta^{1/3}\nu^{2/3}} = \frac{l}{\hat{\nu}^{2/3}}. \tag{3.11}$$

Suppressing all the hats the nondimensional equation is

$$J(\psi, \psi_x) + \psi - \phi = \psi_{xxx}. \tag{3.12}$$

Implicit in (3.12) is the surprising result that all of the streamlines pass through the viscous-inertial boundary layer of width δ_M, even as $\nu \to 0$. Indeed for all the runs examined we found that the first longitude where the meridional velocity changes sign (section D in Figure 7) coincides very closely with $2\pi\delta_M/\sqrt{3}$. This is just the location predicted by the linear Munk solution (see Pedlosky, 1987), assuming that the mass is returned in a Munk boundary layer. We emphasize that the solution is nonlinear and departs strongly from the Munk solution in other respects.

In summary, we suggest that the scaling in (3.9) is appropriate far away from the wall while the scaling in (3.11) applies next to the wall. Notice that (3.12) contains no parameters, so that the scaling (3.11) is "canonical." As long as the meridional scale of the loop, $\mathcal{L}$, is much larger than the scale of the outflow, l, the β-viscous-inertial balance (3.12) obtains near the western boundary. For our pivot run the ratio $\mathcal{L}/l$ is

about 4. The other limit, $\mathcal{L} \ll l$, is the well known Munk solution, in which inertia is negligible.

We emphasize that these are assertions about the inviscid limit, $\nu \to 0$. According to the last relation in (3.11), as viscosity is reduced the length of the loop, $\mathcal{L}$, increases so there is a larger distance over which the small viscosity can act. In fact the area of the loop is of order $\delta_M \mathcal{L} \sim \nu^{-1/3}$. Also the diffusion time across the loop scales as δ_M^2/ν, while the advection time through the loop is $\mathcal{L}\delta_M/\Phi$. The ratio of these two time scales is independent of ν.

Pedlosky suggested this peculiar type of singular limit might give the wave an important dissipative role as $\nu \to 0$. Instead our numerical results suggest that most of the dissipation occurs in the loop, rather than the wave. The wave does become weakly damped as $\nu \to 0$, but we believe that it is best regarded as a local phenomenon resulting from meridional displacement of particles on a β-plane. Potential vorticity transformations take place in the loop, not the wave. In fact, even if the viscous flux of potential vorticity in the wave is $O(1)$, a much larger amount, $O(\nu^{-2/3})$, is needed. This is because as $\nu \to 0$, both the length of the overshoot and that of the plunge increase as $\nu^{-2/3}$. Thus if one holds the center of the outflowing jet fixed at $y = Y$ and reduces ν then eventually it will be necessary to move both the southern boundary farther south and the northern wall farther north so that the loop does not recirculate against either boundary. But the difference between inflowing and outflowing values of potential vorticity on the same streamline must then also increase as $\nu^{-2/3}$ and so must the viscous flux through the streamline.

In Section 4 we provide more details about the potential vorticity transformations in the loop versus the wave. Here we just remark that the large amplitude loop current near the western boundary is a very efficient mechanism for producing Lagrangian potential vorticity changes. High values of potential vorticity acquired in high latitudes by the "overshoot" are then carried southward by the "plunge" and diffused into the northward flowing portion of the current near the inflow region. Thus when fluid with low q initially enters the domain at $y = 0$ there is a flux of high q from the wall and also a flux of high q from the southward flowing branch of the loop current.

e. A remark on the overshoot. The "overshoot" is the northern part of the loop current where $\phi = 0$ and Stewart's constraint, (3.4), is simply $\nu\psi_{xxx}(0, y) = 0$. Thus there is no diffusive flux of potential vorticity through the wall in the overshoot region. Instead diffusion acts only to transfer potential vorticity between the streamlines within the loop. The overshoot must be detached from the wall, else Stewart's constraint would be violated. This separation is not striking in Figures 3, 4 and 5, but is noticeable in the expanded view in Figure 7.

Because the current is detached from the wall the vorticity at the wall is also small.

Thus in the overshoot the momentum integral, (3.7), simplifies to

$$\partial_y \int_0^a v^2\, dx = -\beta \int_0^a \psi\, dx < 0, \tag{3.13}$$

so that the divergence of the momentum flux is balanced by the ageostrophic Coriolis torques. Because the latter is negative the meridional velocity decreases and the overshoot eventually terminates.

4. Potential vorticity transformations

Friction produces significant Lagrangian changes of potential vorticity as particles pass through the domain: low values of q enter in the southwest corner and much higher values leave on the eastern boundary. And while the net advective flux of potential vorticity entering the domain at $y = 0$ vanishes, the advective flux leaving at $x = a$ is

$$\int_0^b u\beta y\, dy = \beta \int_0^b \phi\, dy > 0. \tag{4.1}$$

We noted in the discussion surrounding (3.4) that this advective flux is balanced by the diffusive flux of potential vorticity through the western wall.

These earlier arguments showed how the global potential vorticity budget is balanced, but did not explain how the outer streamlines, which initially absorb all of the viscous flux from the western wall, transfer high potential values vorticity to the inner streamlines.[6]

To visualize the potential vorticity changes which occur as fluid passes through the regional model we use ψ-q scatter plots along the five sections shown in Figure 7. Figures 8 and 9 show a ψ-q scatter plot for run 1. The solid curves are the entry and exit relations and the points come from Sections A, B & C in Figure 8 and from Sections D & E in Figure 9.

A surprising result is that on outer streamlines potential vorticity changes are nonmonotonic. For instance at the top of the overshoot q is greater than the ultimate exit value (see Section D in Fig. 9). Then as the streamline plunges southwards q decreases, so that at the bottom of the first trough (Section E in Fig. 9) q is almost equal to the ultimate exit value. There are only very small changes in q for the remaining five or six visible oscillations in Figure 4.

In contrast, the potential vorticity on inner streamlines changes monotonically from its low entry values to its ultimate high exit value. But the rapidity of these changes is surprising. For instance in Figure 8 we see that at Section B, only 400 km north of the inflow, the ψ-q relation on the inner streamlines is no longer linear.

An obvious explanation for the nonmonotonic potential vorticity changes on outer streamlines is that fluid on these paths must initially absorb all of the viscous flux from

6. By outer streamlines we mean $0 < \psi < \Phi/2$ and by inner streamlines $\Phi/2 < \psi < \Phi$.

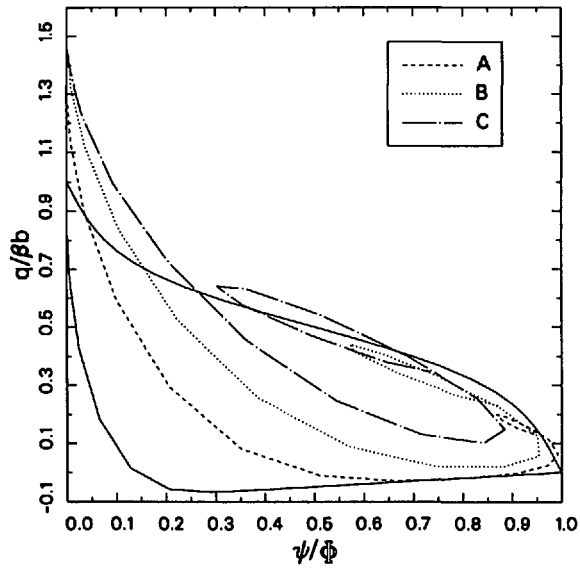

Figure 8. The solid curves are the ψ-q relations of the inflow and outflow. (The linear ψ-q relation in the inflowing inertial boundary current is evident when $\psi > 0.3\ \Phi$.) The broken lines show the ψ-q relations of the three zonal sections from Figure 7. Note how even on Section B, which is only 400 km north of the inflow, some of the inner streamlines have q values in excess of the inflow.

the western boundary. But we are left with the puzzling observation of a very rapid rise of q on the inner streamlines.

A more detailed diagnostic is shown in Figure 10, where potential vorticity, q, planetary vorticity, βy, and the diffusive flux $\nu \nabla q \cdot \mathbf{n}$ on specific streamlines are plotted as a function of arclength, s, ($\mathbf{n}$ is the unit vector normal to the streamline). In accordance with the scaling (3.11) we have normalized the diffusive flux with $\beta\Phi$, and the arclength, s, with $\mathcal{L}$. The potential vorticity and the planetary vorticity are normalized with βb.

In Figure 10a the streamline is $\psi = 0.2\Phi$ and again we note that on this outer streamline the potential vorticity (solid line) at the top of the overshoot exceeds the final exit value. Most of the diffusive flux through the streamline takes place during the northward ascent along the western boundary. The flux in the damped wave region is negligible.

In Figure 10b we pick the inner streamline $\psi = 0.84\Phi$. Most of the diffusive flux through this streamline occurs where the loop current flows southwards. In this region the high values of potential vorticity carried southward from the peak of the overshoot are juxtaposed with the low values of the inflow.

These diagnostics confirm that the largest potential vorticity transformations occur in the loop current near the western boundary. The scaling in (3.11) and (3.12) shows

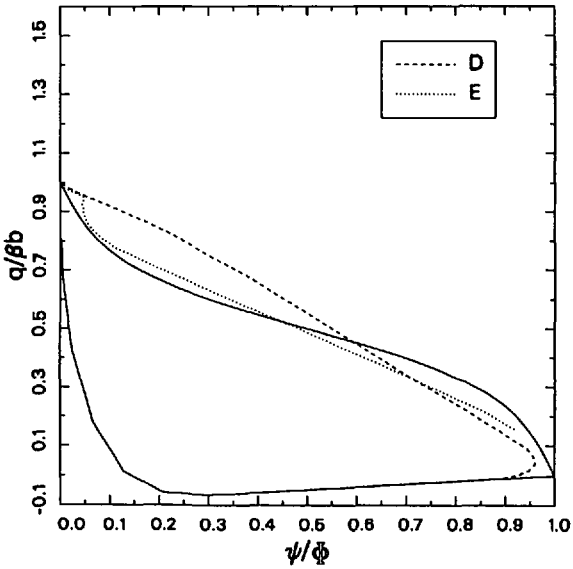

Figure 9. The solid curves are the ψ-q relations of the inflow and outflow. Section D passes through the overshoot and shows that a substantial number of streamlines ($\psi < 0.6\Phi$) have q values in excess of their ultimate outflow values. Note also that on some outer streamlines, such as $\psi < 0.1\Phi$, q has actually decreased between sections C and D. By Section E most streamlines have q values very close to their exit values.

that in the loop inertia, viscosity and planetary vorticity all contend at leading order. By contrast, in the wave region inertia and planetary vorticity approximately balance so that potential vorticity is almost conserved.

5. Conclusions

A primary objective of this paper has been to demonstrate the existence of the damped stationary Rossby wave and document the loop current regime. In the regional numerical model a northward flowing inertial current enters the domain in the southwest corner and separation is induced by specifying an outflow on the eastern boundary, well south of the northern wall. Far from the western wall the flow exhibits the damped stationary Rossby wave described by Moore. However, contrary to the conclusions in Pedlosky (1987), most of the potential vorticity alterations occur at the western boundary, and not in the wave. Taking $\nu \rightarrow 0$ results in a peculiar singular limit: immediately adjacent to the western wall we find a "loop current" with zonal scale $\delta_M \sim \nu^{1/3}$ and a meridional scale which increases as $\nu^{-2/3}$. The ratio of the diffusion time across the loop to the transit time through the loop is independent of ν as $\nu \rightarrow 0$. All the streamlines pass through this region. Thus weak viscosity results in substantial Lagrangian changes in potential vorticity before fluid leaves the loop and enters the wave.

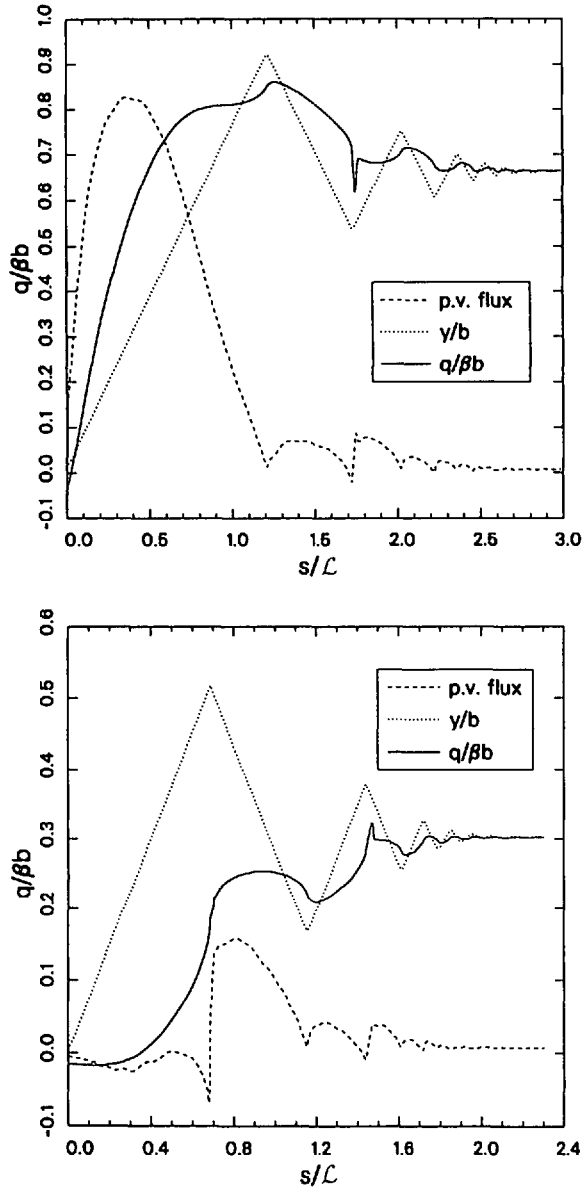

Figure 10. Potential vorticity scaled by βb (solid line), planetary vorticity scaled by βb (dotted line), and nondimensional diffusive flux of potential vorticity, $\nu \nabla q \cdot \mathbf{n}/(\beta\Phi)$ (dashed line) as a function of arclength $s/\mathcal{L}$ on a streamline for run 1. (a) An outer streamline: $\psi = 0.2\Phi$. (b) An inner streamline: $\psi = 0.84\Phi$.

Because of the geometry of the loop the fluid entering the domain is diffusively invaded by high potential vorticity from both the wall on the left and the loop current on the right. This is an example of upstream influence mediated by viscosity, even in the inviscid limit. The potential vorticity distribution in the southward flowing branch of the loop is determined by the imposed outflow on the eastern wall, and by diffusive interaction with the northward flowing branch. This information is communicated to the entering fluid before the latitude band at which the outflow is imposed.

The loop current is an alternative regime to inertial recirculation through which potential vorticity is transformed from the low values entering the domain to the high values of the outflow. The main difference between the two regimes is that the former does not produce increased transport. We believe that geometry is the main factor determining whether recirculation or the loop current is realized. If the northward boundary current comes in contact with a solid northern wall, or, presumably, with a southward flowing current of comparable strength, then inertial recirculation is obtained. When recirculation occurs its strength and size increase with decreasing ν, and potential vorticity transformations take place in the viscous layer between the gyre and the northern wall.

The relevance of the viscous-inertial loop current to oceanic observations is unclear because it may be unstable to time dependent perturbations. (The solutions in this article were obtained using Newton's method and we can conclude nothing about their stability as ν is decreased.) Nevertheless the loop current found here might capture some of the dynamical processes taking place in southern ocean western boundary currents, i.e. the East Australian Current and the Aghulas Current. The absence of a (southern) wall, or of another western boundary current flowing in the opposite direction, distinguishes these southern ocean currents from the Gulf Stream. In the North Atlantic there is evidence from eddy resolving numerical simulations (Thompson and Schmitz, 1989) that the interaction of the southwestward flowing Deep Western Boundary Current with the Gulf Stream gives rise to inertial recirculation both to the north and south of the separated Gulf Stream. Instead the East Australian Current (Boland and Church, 1981) overshoots its latitude of separation in a highly time dependent fashion and exhibits a train of nonpropagating damped Rossby waves as it flows eastward across the Tasman Sea. In this system there is no counterflowing boundary current, analogous to the Deep Western Boundary Current, and so there is no inertial recirculation associated with the separated East Australia Current.

The Aghulas current system is another point of comparison complicated by the geometry of the coastline: the boundary terminates at the tip of South Africa. We speculate that the Aghulas retroflection is an example of an inertial-viscous overshoot like that in the East Australian Current system and in Figure 3. The importance of both viscosity and inertia in this region is supported by the simulations of Boudra and Chassignet (1988) and this agrees with the balance we emphasized in the discussion surrounding (3.13). In this bulk conservation equation for meridional momentum there

is no viscous term yet viscosity has an essential role in distributing momentum and vorticity across streamlines.

Acknowledgments. We thank Glenn Ierley for generously providing the numerical code and the diagnostic routines. PC is supported by the National Science Foundation and the Italian National Research Council (CNR). WRY is supported by the National Science Foundation and the Office of Naval Research. This work began at the 1989 Woods Hole Summer Study Program in Geophysical Fluid Dynamics. The numerical calculations were performed at the San Diego Supercomputer which is supported by the National Science Foundation.

REFERENCES

Batchelor, G. K. 1967. An Introduction to Fluid Dynamics, Cambridge University Press, 615 + xvii pp.

Blandford, R. R. 1971. Boundary conditions in homogeneous ocean models. Deep-Sea Res., *18,* 739–751.

Boland, F. M. and J. A. Church. 1981. The East Australian Current 1978. Deep-Sea Res., *28,* 937–958.

Böning, C. 1986. On the influence of frictional parameterization in wind-driven ocean circulation models. Dyn. Atm. Oceans, *10,* 63–92.

Boudra, D. B. and E. P. Chassignet. 1988. Dynamics of Aghulas retroflection and ring formation in a numerical model. Part I: The vorticity balance. J. Phys. Oceanogr., *18,* 280–303.

Bryan, K. 1963. A numerical investigation of a nonlinear model of a wind-driven ocean. J. Atm. Sci., *20,* 594–606.

Cessi, P., G. R. Ierley and W. R. Young. 1987. A model of the inertial recirculation driven by potential vorticity anomalies. J. Phys. Oceanogr., *17,* 1640–1652.

Charney, J. G. 1955. The Gulf Stream as an inertial boundary layer. Proc. Natl. Acad. Sci., *41,* 731–740.

Condie, R. V. 1989. Barotropic boundary layer separation regimes, *in* Proceedings of the 1989 Woods Hole Oceanographic Institution Summer Study Program in Geophysical Fluid Dynamics, Woods Hole Oceanogr. Inst. Techn. Rep., WHOI-89-54.

Hendershott, M. C. 1987. Single layer models of the general circulation, *in* The General Circulation of the Ocean, H. Abarbanel and W. R. Young, eds., Springer-Verlag, 291 pp.

Ierley, G. R. 1987. On the onset of inertial recirculation in barotropic general circulation models. J. Phys. Oceanogr., *17,* 2366–2374.

Ierley, G. R. and O. G. Ruehr. 1986. Analytic and numerical solutions of a nonlinear boundary layer problem. Stud. Appl. Math., *75,* 1–36.

Ierley, G. R. and W. R. Young. 1988. Inertial recirculation in a β-plane corner. J. Phys. Oceanogr., *18,* 683–689.

—— 1990. Viscous instabilities in the western boundary layer. J. Phys. Oceanogr., (in press).

Il'in, A. M. and V. M. Kamenkovich. 1964. The structure of the boundary layer in the two dimensional theory of ocean currents. (In Russian.) Okeanologiya, *5,* 756–769.

Mallier, R. 1989. The parametric model of western boundary layer outflow, *in* Proceedings of the 1989 Woods Hole Oceanographic Institution Summer Study Program in Geophysical Fluid Dynamics, Woods Hole Oceanogr. Inst. Techn. Rep., WHOI-89-54.

Moore, D. W. 1963. Rossby waves in ocean circulation. Deep-Sea Res., *10,* 735–747.

Morgan, G. W. 1956. On the wind driven ocean circulation. Tellus, *8,* 301–320.

Moro, B. 1988. On the nonlinear Munk model. I. Steady flows. Dyn. Atm. Oceans, *12,* 259–287.

Munk, W. H. 1950. On the wind-driven ocean circulation. J. Meteorol., *7,* 79–93.

Panteleev, M. C. 1985. The influence of friction on the character of the barotropic wind driven circulation. (In Russian.) Izvestia POLYMODE, *15,* 34–39.

Pedlosky, J. P. 1987. Geophysical Fluid Dynamics, 2nd ed. Springer Verlag, 710 + xiv pp.

Schlichting, H. 1979. Boundary-Layer Theory, 7th ed. McGraw-Hill, 817 + xxii pp.

Stewart, R. W. 1964. Influence of friction on inertial models in oceanic circulation, *in* Studies on Oceanography: Papers dedicated to Professor Hidaka in commeration of his 60'th birthday. K. Yoshida, ed., Tokyo University, Geophysical Institute.

Thompson, J. D. and W. J. Schmitz, Jr. 1989. A limited-area model of the Gulf Stream: design, initial experiments and model-data intercomparison. J. Phys. Oceanogr., *19,* 791–814.

Received: *10 July, 1990;* revised: *23 October, 1990.*